

Thickness effects on the physical characterization of nanostructured CuO thin films for hydrogen gas sensor

E. H. Hadia^a, F. H. Jasim^a, S. S. Chiad^a, K. N. Hussein^{b,*}, N. F. Habubi^c,
Y. H. Kadhim^d, M. Jadan^{e,f}

^a*Department of Physics, College of Education, Mustansiriyah University, Iraq,*

^b*Department of Radiology, Al-Manara College for Medical Science, Iraq*

^c*Department of Radiation and Sonar Technologies, Alnukhba University College, Iraq*

^d*Department of Optics Techniques, Al-Mustaqbal University College, Babylon, Iraq*

^e*Department of Physics, College of Science, Imam Abdulrahman Bin Faisal University, P.O. Box 1982, 31441 Dammam, Saudi Arabia*

^f*Basic and Applied Scientific Research Center, Imam Abdulrahman Bin Faisal University, P.O. Box 1982, 31441 Dammam, Saudi Arabia*

In these studies, radio frequency (RF) magnetron sputtering was used to produce nanostructured CuO thin films on glass bases with different thicknesses of (250, 300, and 350 nm). X-ray diffraction (XRD) analysis of these films revealed a polycrystalline structure with a preferred peak along the (111) plane. The Scherrer formula was used to compute the grain size. It was found that the average grain sizes are 10.78 nm, 11.36 nm, and 11.84 nm for film thicknesses of 250, 3000, and 300 nm, respectively, while the dislocation density and strain values decline. The surface roughness decreased from 9.30 nm to 4.71 nm as the thickness increased, according to atomic force microscopy (AFM) data. As the thickness of the film grew, the root mean square (RMS) roughness likewise decreased from 9.18 nm to 4.29 nm. The homogenous, semi-spherical structure comprises uniformly distributed particles, as demonstrated by SEM images. The optical properties of the grown films showed that the absorption coefficient considerably increased with film thickness. Transmittance, band gap, refractive index, and extinction coefficient all decrease with increasing film thickness. The hydrogen gas measurements, indicated a reduction in sensitivity as the thickness and gas concentration increased at 30°C.

(Received February 2, 2024; Accepted May 9, 2024)

Keywords: CuO, sensing, Thickness, Structural, Morphological

1. Introduction

In numerous industries, several semiconductors are either in advanced usage or being explored for applications, such as photovoltaic cells [1], antibacterial activities [2], sensing [3,4], magnetic storage media [5], and supercapacitors [6]. Nanostructured CuO has a wide band gap of (1.4-3.1 eV) [7]. Materials like CuO and Cu₂O are generally considered p-type semiconductors, making them potentially helpful for making junction devices like pn junction diodes [8]. The components of cupric oxide are plentiful and non-toxic. These benefits have drawn much interest to their application in several fields, including photovoltaic devices and power sources [9]. Several methods are employed to deposit nanostructured CuO films, like CVD [10,11], electrodeposition technique [12,13], reflux condensation [14], SILAR [15], sol-gel spin-coating process [16], spray pyrolysis [17], thermal oxidation [18], and magnetron sputtering [19-21]. This work focused on the synthesis of nanostructured copper oxide films of various thicknesses by RF magnetron sputtering and studied their XRD, AFM, and UV-VIS spectroscopy to obtain the structures and optical characteristics of these films in order to use them for hydrogen gas sensors.

* Corresponding author: karrar.noor.h@gmail.com

<https://doi.org/10.15251/DJNB.2024.192.717>

2. Experimental

CuO films were deposited using RF magnetron sputtering technique. A CuO target with a purity of 99.99%, before starting, an oxide layer was removed from the target by pre-sputtering it in an argon environment. The turbomolecular pump evacuated the sputtering chamber to a pressure of 5×10^{-5} mbar. Thin films were grown on a glass, which served as the substrate. By employing XRD, the crystalline characteristics of the CuO films are examined. A weighing method was used to determine the film thickness, which was (250, 300, and 350) nm. The XRD method was applied to explore how the crystal structure behaves. AFM images were captured for morphological analyses utilising the tapping mode of the Nanoscope IIIa scanning probe microscope controller. The morphology of the deposited thin film was employed using a Scanning electron microscope SEM, Shimadzu 3101 PC Spectrometer data for optical transmission in the (300 - 900 nm) were used for optical analysis. Gas sensing measurements were conducted using the testing system depicted in Figure (1)

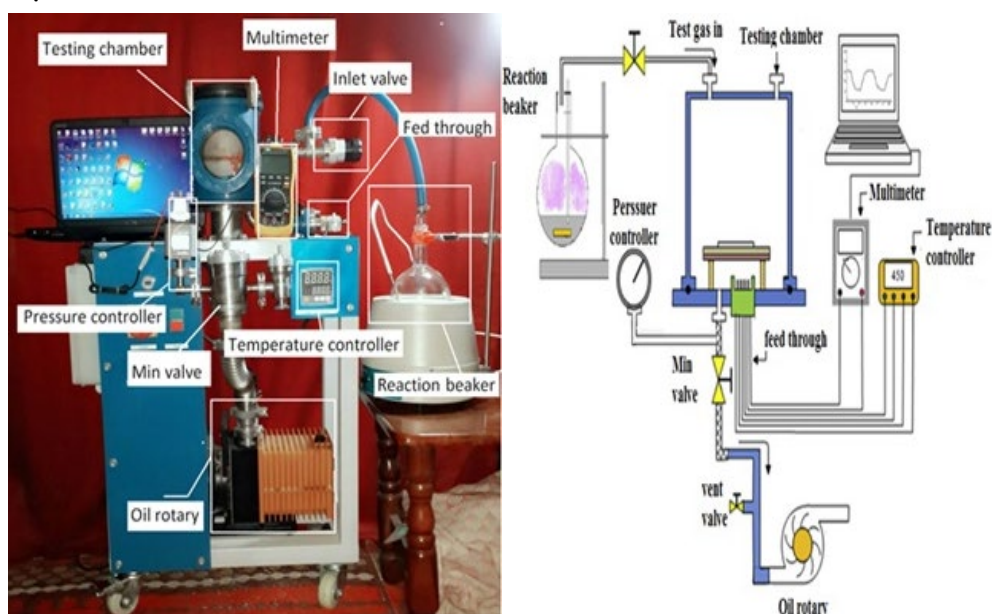


Fig. 1. Gas sensor testing system.

3. Results and discussion

3.1. XRD

The X-ray diffraction (XRD) patterns for different film thicknesses (250 nm, 300 nm, and 350 nm) are illustrated in Figure 2. In comparison to the standard JCPDS card No. (05-0661), the analysis revealed that the grown films exhibit a polycrystalline monoclinic structure. This finding aligns with the results reported by Mageshwari et al. [14]. The identified crystallographic planes include (110), (111), (020), and (220), with corresponding peaks observed at ($2\theta=32.25^\circ$, 38.37° , 53.43° , and 65.43°), respectively. These results are in accordance with previous studies [22, 23], confirming the consistency of the observed crystallographic characteristics with established literature in the field. Debye-Scherrer's formula was employed to evaluate crystallite size (D) is given by [24, 25]:

$$D = \frac{0.94\lambda}{\beta \cos\theta} \quad (1)$$

where θ is the Bragg angle, β is FWHM, and λ is the wavelength. Since increasing thickness results lead to increase in the grain size, the increase in film thickness could cause these modifications, resulting in an enhancement in film crystallinity, rearranging of atoms, and the elimination of defects [26]. Similar research for thin films with a thickness of 350 nm has been published. [27].

Dislocation density (δ) is calculated from Eq. (2) [28, 29]:

$$\delta = \frac{1}{D^2} \quad (2)$$

strain (ϵ) is calculated from the following Eq. (3) [30-32]:

$$\epsilon = \frac{\beta \cos \theta}{4} \quad (3)$$

According to Table 1, dislocation density and strain reduced as thickness increased. As the thickness increases, the peak locations remain unchanged. Thin CuO films with 250 nm and 350 nm thickness have the same lattice constant and volume cell. This behavior matches well with [18]. Figure (3) displays FWHM, D , δ and ϵ versus different thicknesses.

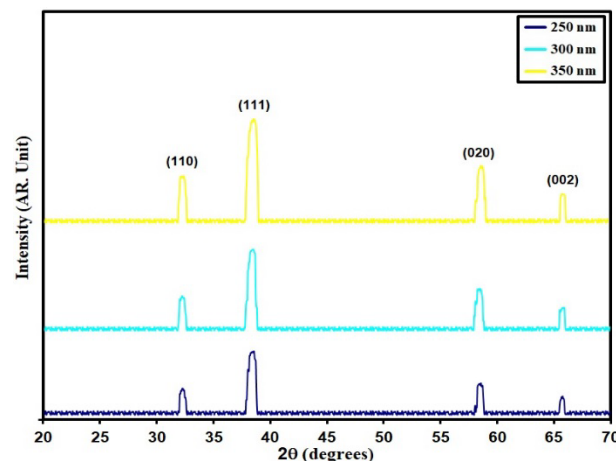


Fig.2. XRD of grown films

Table 1. XRD parameters and energy gap of grown films.

Thickness (nm)	2 θ ($^{\circ}$)	(hkl) Plane	FWHM ($^{\circ}$)	E_g (eV)	D (nm)	δ ($\times 10^{14}$) (lines/m 2)	ϵ ($\times 10^{-4}$)
250	38.37	111	0.78	2.54	10.78	85.92	32.13
300	38.35	111	0.74	2.49	11.36	77.36	30.49
350	38.30	111	0.71	2.41	11.84	71.33	29.26

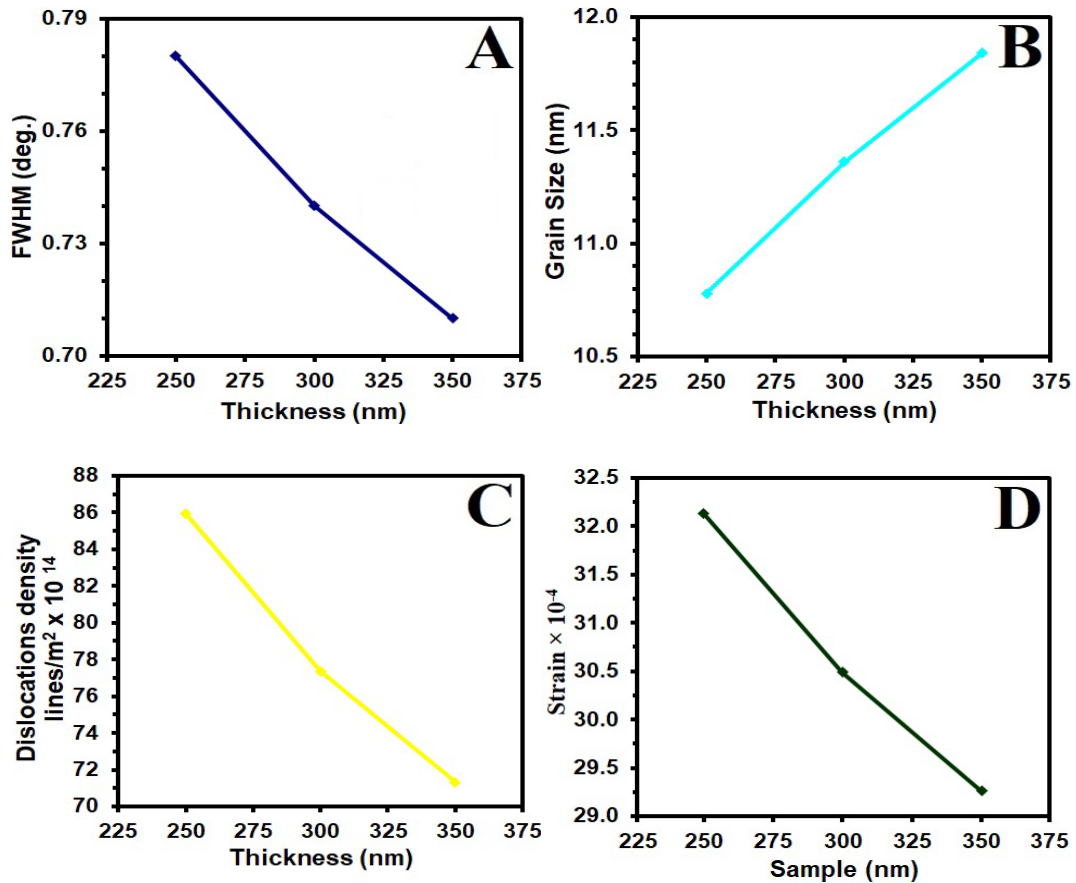


Fig. 3. XRD parameters of CuO films.

3.2. AFM analysis

The morphology of the material was examined using atomic force microscopy (AFM) [10]. The obtained data, including root mean square (RMS), surface roughness average (R_s), and particle size (P_{av}), are presented in Table 4. As the thickness increased, P_{av} demonstrated a decrease, indicating a correlation between thickness and particle size. Additionally, RMS exhibited a decline from 9.18 nm to 4.29 nm at a thickness of 300 nm, mirroring the trend observed in R_s , which decreased from 9.30 nm to 4.71 nm. These findings suggest that an increase in thickness is associated with a reduction in both surface roughness and particle size, as indicated by the recorded values in Table 4.

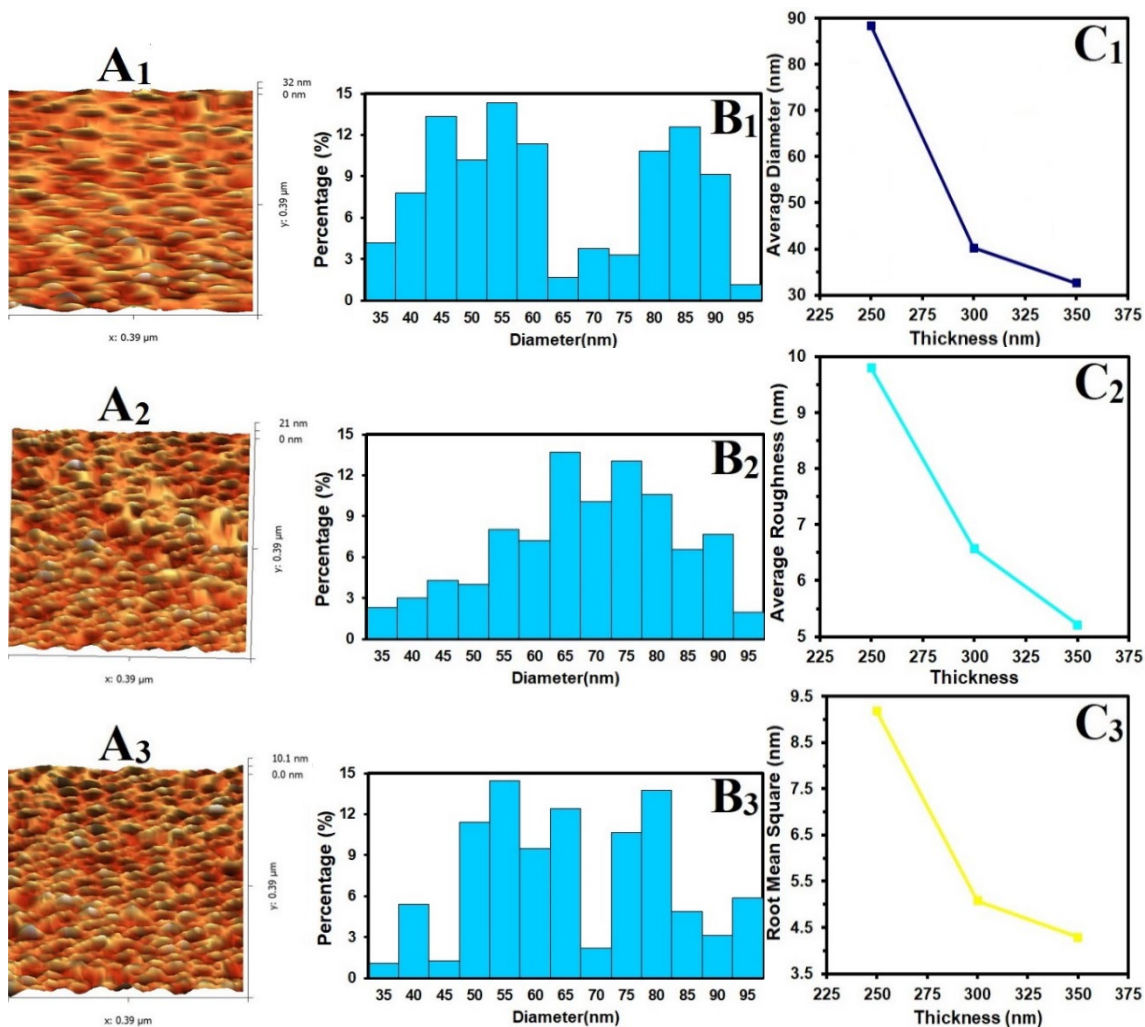


Fig. 4. AFM information of CuO films.

Table 2. AFM parameters of (CuO) thin film with different thicknesses.

Thickness (nm)	P_{av} (nm)	R_s (nm)	RMS (nm)
250	88.4	9.30	9.18
300	40.2	6.07	5.08
350	32.6	4.71	4.29

3.3. SEM analysis

The surface morphology is depicted in Figure 5, revealing a notable presence of uniformly distributed particles forming a homogeneous, semi-spherical structure. A noticeable trend is observed, wherein the grain size increases with thickness, varying from 26.67 to 44.9 nm. This thickness-dependent increase in grain size can be attributed to improved nucleation and growth processes as the film thickness expands. The larger and more well-defined grains observed with increasing thickness are indicative of an enhanced crystalline structure [21].

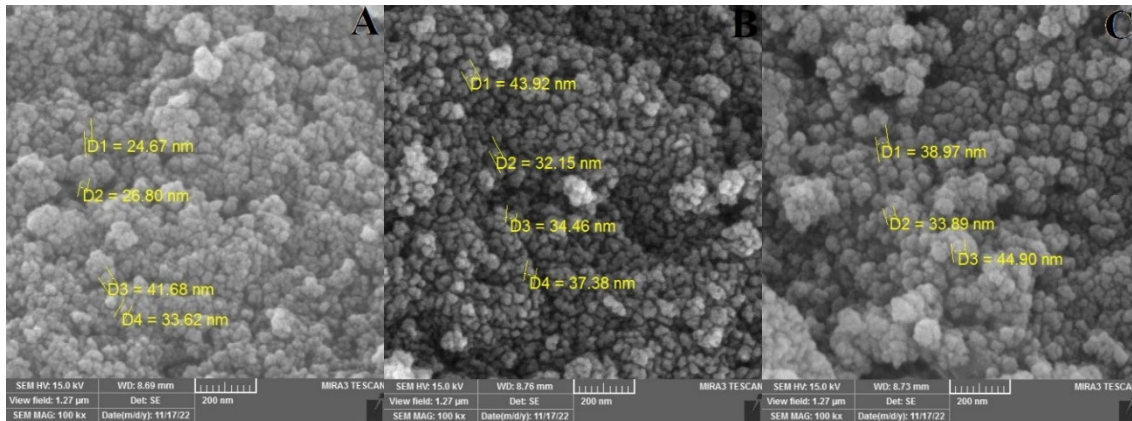


Fig. 5. SEM images of CuO: A 250 nm, B 300 nm, C 350 nm.

3.4. Optical properties

Figure (6) shows the absorbance (A) of samples of varied thicknesses (100, 150, and 200 nm) as measured by a UV-Vis scanning spectrophotometer. For all thicknesses, the absorption of CuO film reduced as the wavelength increased, well matched with reference [33]. The films' ability to absorb light can be reduced when crystallite size decreases with increasing thickness [8]. Additionally, transmittance (T) is recorded via Eq (4) [34-36]:

$$A = 2 - \log_{10} (\% T) \quad (4)$$

T of CuO films increased with increasing wavelength for all thicknesses, but T decreased as the thickness increased, as shown in Figure (7). With increasing Thickness, T in the visible range (340-650 nm) increases from 11% to 88% [12].

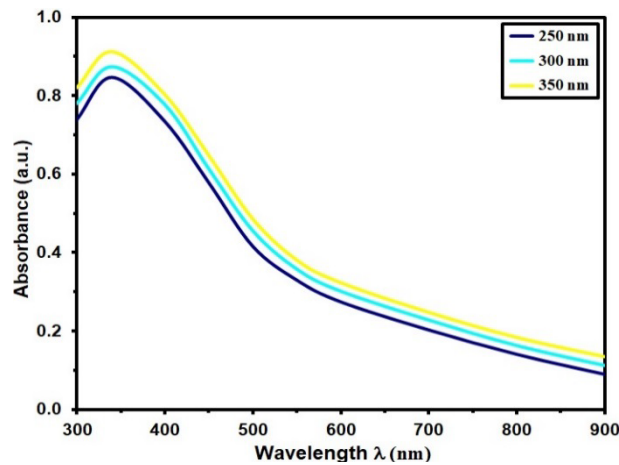


Fig. 6. Absorbance of the CuO films.

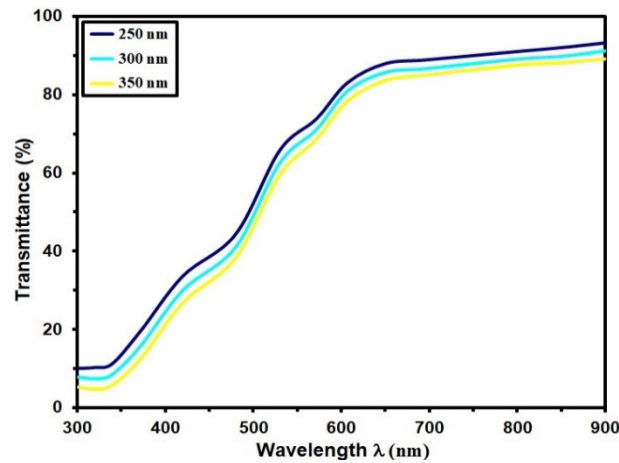


Fig. 7. T of CuO films.

A formula was developed to calculate the absorption coefficient (α) via Eq. (5) [37-39]:

$$\alpha = (2.303 \times A)/d \quad (5)$$

where d is film thickness. The transmittance increases with increasing photon energy ($h\nu$), consistent with published research. Figure (8) depicts the variation of α , (at a rate of 10^4 cm^{-1}) is assigned to direct transitions. [40]

The direct optical band gap E_g is calculated via Tauc in Eq. (6) [41-43]:

$$(\alpha h\nu) = A(h\nu - E_g)^n \quad (6)$$

where A is always the same. Figure (9) depicts the fluctuation of $(\alpha h\nu)^2$ with photon energy ($h\nu$) of CuO films. This Figure displays the direct allowed transition predominates. These results agreed with reference [2], and the estimated E_g values range from 2.54 to 2.41 eV with increasing thickness. The improvements in crystallinity and morphological modifications, as well as changes in the atomic distances and grain size, can be linked to the narrowing band gap that occurs with increasing thickness. Furthermore, the band gap may be reduced due to the localised states in the band structure merging with the band boundaries as the film thickness increases. This is because the band gap decreases as the film thickness increases. These findings align perfectly with the findings of our XRD analysis [18].

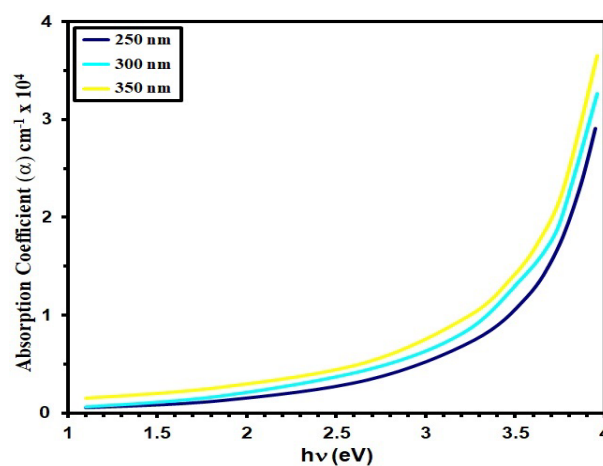


Fig. 8. α Vs $h\nu$ of CuO films.

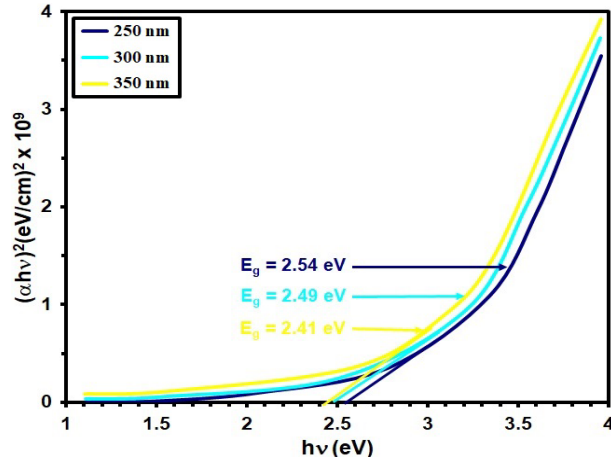


Fig. 9. $(\alpha h\nu)^2$ of grown films.

The extinction coefficient (k) value is obtained via the following [44-46]:

$$k = \frac{\alpha\lambda}{4\pi} \tag{7}$$

The Figure shows variations in k with wavelength (10). Since crystal development is slowed down as thickness increases, it is seen that n decreases with Thickness [17]. These films' relatively low extinction coefficients reveal the particle size and surface's uniformity and smoothness. The reduction in extinction coefficient with thickness shows lower absorption in thicker materials. [15].

The refractive index (n) was determined using the following [47-49]:

$$n = \left(\frac{1 + R}{1 - R}\right) + \sqrt{\frac{4R}{(1 - R)^2} - k^2} \tag{8}$$

where R is the reflectivity, Figure (11) shows that the films deposited at 350 nm had the greatest refractive index values, while those formed at a thickness of 250 nm had the lowest values (3.09) at a wavelength of 540 nm (3.20). The refractive indices of the deposited materials fell exponentially as wavelengths increased in the (550-900 nm) range, indicating limited light absorption at long wavelengths. [50]

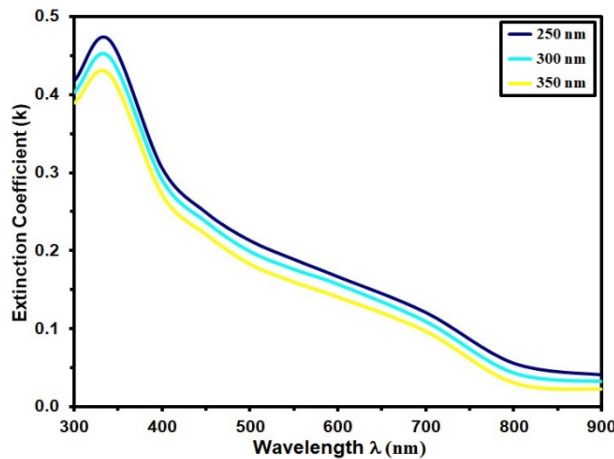


Fig. 10. k of grown films.

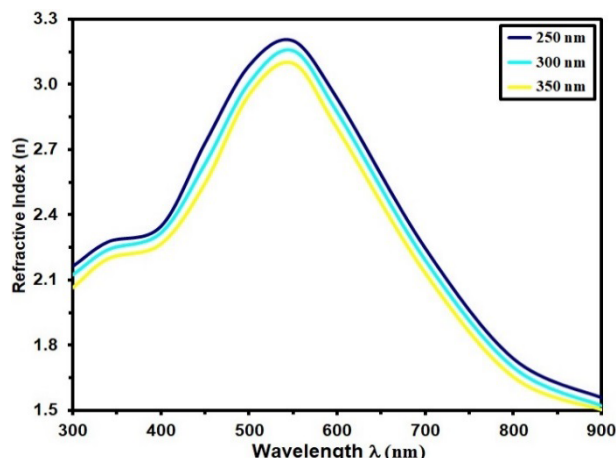


Fig. 11. n of the grown films.

3.4. Gas sensing characteristics

Figure (12) illustrates the correlation between resistance over time of CuO films with different thicknesses (250, 330, and 350 nm) under varying 500 ppm of hydrogen gas at an operational temperature of 30°C. The adsorption of hydrogen molecules (H_2) on the surface induces an oxidation process. Through this action, some O^{2+} ions are removed from the surface, freeing the oxygen atoms' bonded electrons. After that, these liberated electrons return to the conduction band [51, 52], increasing the resistance value and enhancing the potential barrier under these conditions [54]. Notably, the CuO film with a thickness of 350 nm exhibits the highest resistance to gas flow, concurrently displaying the largest ΔR , which is directly proportional to film sensitivity, as per the following relationship [53, 54].

$$Sensitivity = \frac{\Delta R}{R_g} = \left| \frac{R_g - R_a}{R_g} \right| \times 100 \% \quad (9)$$

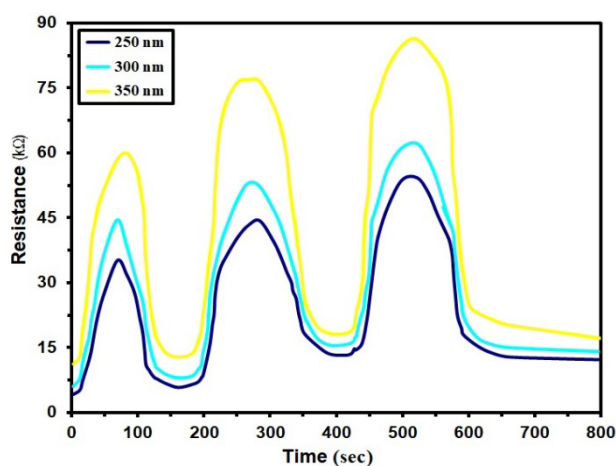


Fig. 12. Dynamic resistance change of CuO Films at 500 ppm of H_2 gas.

Figure (13) depicts the sensitivity plots corresponding at varying thicknesses (250, 330, and 350 nm) after exposure to hydrogen gas. The results indicate a decrease in sensitivity with an increase in thickness, attributed to the elevated electrical resistance of the film caused by the recombination process between charge carriers (holes) and electrons released from oxygen [55]. The sensitivity diminishes from 53% to 27% for 500 ppm, 44% to 22% for 400 ppm, and 38% to 18% for 300 ppm for the respective thicknesses (250, 330, and 350 nm).

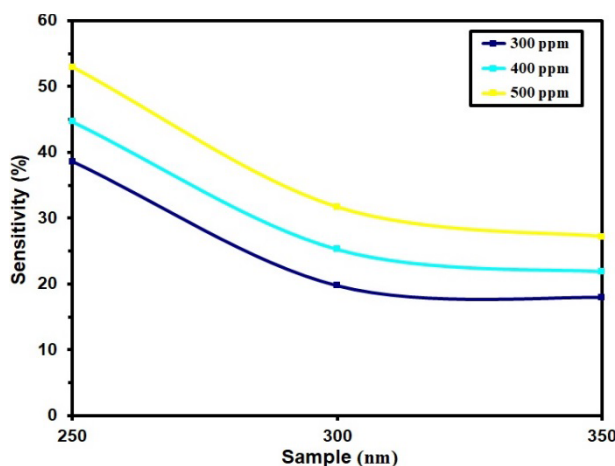


Fig. 13. Sensitivity of CuO films at different content of H₂ gas.

4. Conclusion

Our study examined the morphology, optical properties, and polycrystalline nature of CuO thin films grown by (RF) magnetron sputtering. We calculated the average grain size from the XRD data and found that it is (10.78, 11.36, and 11.84) nm for thickness (250, 300, and 350) nm, respectively. AFM roughness decreased from 9.18 to 4.29 nm as thickness increased from (250-350 nm). SEM images show that the grain size increases with thickness; the grain sizes range from 26.67 to 44.9 nm. It was discovered that transmittance declines with increasing thickness while absorption rises for the wavelength range. The optical energy gap was (2.54 eV to 2.41 eV). The best sensitivity for thickness 350 nm CuO was (53%) at an operating temperature of (150 °C) for 300 ppm gas concentration.

Acknowledgements

This work is propped by Mustansiriyah University ([www. uomustansiriyah.edu.iq](http://www.uomustansiriyah.edu.iq)) and Alnukhba University College.

References

- [1] B. Boudjema, R. Daira, A. Kabir, R. Djebien, Materials Science Forum, Trans Tech Publ, 895, 33-36 (2017); <https://doi.org/10.4028/www.scientific.net/MSF.895.33>
- [2] M. Asadi, S. M. Rozati, Mater. Sci. Pol., 35 (2) 355-361 (2017); <https://doi.org/10.1515/msp-2017-0054>
- [3] L. J. Meenakshi, B. R. Aswathy, P. K. Manoj, AIP Conf. Proc., 2287 (11), 698-701 (2020); <https://doi.org/10.1063/5.0029961>
- [4] G. Madec, P. Delecluse, M. Imbard, et C. Levy, Notes du Pôle Modélisation, Inst. Pierre Simon Laplace, 14 (4), (2014) ; <https://doi.org/10.2478/adms-2014-0021>
- [5] S. K. Muhammad, M. O. Dawood, N. Y. Ahmed, E. S. Hassan, N. F. Habubi, S. S. Chiad, Journal of Physics: Conference Series, 1660 (1), 012057 (2020); <https://doi.org/10.1088/1742-6596/1660/1/012057>
- [12] R. D. Prabu et al., Mater. Sci. Semicond. Process., 74, 129-135 (2018); <https://doi.org/10.1016/j.mssp.2017.10.023>

- [7] A. O. Ibadon, P. Fitzpatrick, Heterogeneous Photocatalysis: Recent Advances and Applications, 12, 189-218 (2013); <https://doi.org/10.3390/catal3010189>
- [8] F. H. Jasim, H. R. Shakir, S. S. Chiad, N. F. Habubi, Y. H. Kadhi, Jadan, M., Digest Journal of Nanomaterials and Biostructures, 18(4), 1385–1393 (2023); <https://doi.org/10.15251/DJNB.2023.184.1385>
- [9] M. T. S. Nair, L. Guerrero, O. L. Arenas, P. K. Nair, Appl. Surf. Sci., 150 (1) 143-151 (1999); [https://doi.org/10.1016/S0169-4332\(99\)00239-1](https://doi.org/10.1016/S0169-4332(99)00239-1)
- [10] F. A. Jasima, Z. S. A. Mosa, N. F. Habubi, Y. H. Kadhim, S. S. Chiad, Digest Journal of Nanomaterials and Biostructures, 18 (3), 1039–1049 (2023); <https://doi.org/10.15251/DJNB.2023.183.1039>
- [11] I. A. Abbas, S. Q. Hazaa, AIP Conference Proceedings, 2307, 020037 (2020); <https://doi.org/10.1063/5.0033226>
- [12] A. J. Kadhim, I. A. Abbas, Nano Biomedicine and Engineering, 14(4), 360–366 (2022); <https://doi.org/10.5101/nbe.v14i4.p360-366>
- [13] Y. Li, J. Liang, Z. Tao and J. Chen, Mater. Res. Bull, 43, 2380 (2008); <https://doi.org/10.1002/aenm.200800795>
- [14] K. Mageshwari, D. Nataraj, T. Pal, R. Sathyamoorthy, J. Park, J. Alloys Compd. 625, 362 (2015); <https://doi.org/10.1016/j.jallcom.2014.11.109>
- [15] K. Mageshwari, R. Sathyamoorthy, Mater. Sci. Semicond. Process., 16, 337 (2013); <https://doi.org/10.1016/j.mssp.2012.09.016>
- [15] M.H. Kabir, H. Ibrahim, M.M. Billah, AIP Conference Proceedings 2324, 030007 (2021); <https://doi.org/10.1063/5.0037501>
- [17] Kumar, A. S. K. Perumala, P. Thirunavukkarasu, Optoelec. Advan. Mater. –Rapid Commun. 4 (6), 831 – 833 (2010); <https://doi.org/10.3390/coatings11111392>
- [18] Samarasekara, P. “Characterization of low cost P-Cu₂O/N-CuO junction” Physics, 2 (4), 3 (2010); <https://doi.org/10.1016/j.solmat.2010.11.015>
- [19] M. Petrantoni, C. Rossi, L. Salvagnac, V. Conedera, A. Estève, C. Tenailleau, P. Alphonse, Y.J. Chabal, J. Appl. Phys. 108 (2010). <https://doi.org/10.1063/1.3498821>
- [20] H. Search, C. Journals, A. Contact, M. Iopscience, I. P. Address, Journal of Physics: Condensed Matter, 18, 2417 (2006); <https://doi.org/10.1088/0953-8984/18/8/007>
- [21] Pletea, M.; Bruckner, W.; Wendrock, H.; Kaltfen, R. J. Appl. Phys. 97, 054908 (2005); <https://doi.org/10.1063/1.1858062>
- [22] N. N. Jandow, M. S. Othman, N. F. Habubi, S. S. Chiad, K. A. Mishjil, I. A. Al-Baidhany, Materials Research Express, 6 (11), (2020); <https://doi.org/10.1088/2053-1591/ab4af8>
- [23] M. S. Othman, K. A. Mishjil, H. G. Rashid, S. S. Chiad, N. F. Habubi, I. A. Al-Baidhany, Journal of Materials Science: Materials in Electronics, 31(11), 9037-9043 (2020); <https://doi.org/10.1007/s10854-020-03437-0>
- [34] E. S. Hassan, K. Y. Qader, E. H. Hadi, S. S. Chiad, N. F. Habubi, K. H. Abass, Nano Biomedicine and Engineering, 12(3), pp. 205-213 (2020); <https://doi.org/10.5101/nbe.v12i3.p205-213>
- [25] E. H. Hadi, D. A. Sabur, S. S. Chiad, N. F. Habubi, K. H. Abass, Journal of Green Engineering, 10 (10), 8390-8400 (2020); <https://doi.org/10.1063/5.0095169>
- [26] R. Daira B. Boudjema, M. Bououdina, M. S. Aida, Applied Science, (2023); <https://doi.org/10.3390/app13148193>
- [27] K. S. Sharba, A.S. Alkelaby, M. D. Sakhil, K. H. Abass, N. F. Habubi, S.S. Chiad, NeuroQuantology, 18 (3), 66-73(2020); <https://doi.org/10.14704/NQ.2020.18.3.NQ20152>
- [28] M. D. Sakhil, Z. M. Shaban, K. S. Sharba, N. F. Habub, K. H. Abass, S. S. Chiad, A. S. Alkelaby, NeuroQuantology, 18 (5), 56-61 (2020); <https://doi.org/10.14704/nq.2020.18.5.NQ20168>

- [29] S. D. Al Ghamdi, A. O. M. Alzahrani, M. S. Aida, M. S. Abdel-wahab, J. Mater. Sci. Mater. Electron., vol. 33, no 18, p. 14702-14710, 2022 ; <https://doi.org/10.1007/s10854-022-08390-8>
- [30] Khadayeir, A. A., Hassan, E. S., Mubarak, T. H., Chiad, S.S., Habubi, N. F., Dawood, M.O., Al-Baidhany, I. A., Journal of Physics: Conference Series, 1294 (2) 022009(2019); <https://doi.1088/1742-6596/1294/2/022009>
- [31] N. Y. Ahmed, B. A. Bader, M. Y. Slewa, N. F. Habubi, S. S. Chiad, NeuroQuantology, 18(6), 55-60 (2020); <https://doi.org/10.1016/j.jlumin.2021.118221>
- [32] A. J. Ghazai, O. M. Abdulmunem, K. Y. Qader, S. S. Chiad, N. F. Habubi, AIP Conference Proceedings 2213 (1), 020101 (2020); <https://doi.org/10.1063/5.0000158>
- [33] S. Kose, F. Atay, V. Bilgin, I. Akyuz, Materials Chemistry and Physics, 111, 351-358 (2008); <https://doi.org/10.1016/j.matchemphys.2008.04.025>
- [34] S. S. Chiad, H. A. Noor, O. M. Abdulmunem, N. F. Habubi, M. Jadan, J. S. Addasi, Journal of Ovonic Research, 16 (1), 35-40 (2020). <https://doi.org/10.15251/JOR.2020.161.35>
- [35] H. T. Salloom, E. H. Hadi, N. F. Habubi, S. S. Chiad, M. Jadan, J. S. Addasi, Digest Journal of Nanomaterials and Biostructures, 15 (4), 189-1195 (2020); <https://doi.org/10.15251/DJNB.2020.154.1189>
- [36] H. A. Hussin, R. S. Al-Hasnawy, R. I. Jasim, N. F. Habubi, S. S. Chiad, Journal of Green Engineering, 10(9), 7018-7028 (2020); <https://doi.org/10.1088/1742-6596/1999/1/012063>
- [37] Chiad, S.S., Noor, H.A., Abdulmunem, O.M., Habubi, N.F., Journal of Physics: Conference Series 1362(1), 012115 (2019); <https://doi.org/10.1088/1742-6596/1362/1/012115>
- [38] A. A. Khadayeir, R. I. Jasim, S. H. Jumaah, N. F. Habubi, S. S. Chiad, Journal of Physics: Conference Series, 1664 (1) (2020); <https://doi.org/10.1088/1742-6596/1664/1/012009>
- [39] R. S. Ali, N. A. H. Al Aaraji, E. H. Hadi, N. F. Habubi, S. S. Chiad, Journal of Nanostructures this link is disabled, 10(4), 810–816 (2020); <https://doi:10.22052/jns.2020.04.014>
- [40] F. Aksoy, G. Akgul, N. Yildirim, H. Emrah, Mater. Chem. Phys., vol. 147, no 3, p. 987-995, 2014; <https://doi.org/10.1016/j.matchemphys.2014.06.047>
- [41] S. S. Chiad, A. S. Alkelaby, K. S. Sharba, Journal of Global Pharma Technology, 11 (7), 662-665, (2020); <https://doi.org/10.1021/acscatal.1c01666>
- [42] R. S. Ali, M. K. Mohammed, A. A. Khadayeir, Z. M. Abood, N. F. Habubi and S. S. Chiad, Journal of Physics: Conference Series, 1664 (1), 012016 (2020); <https://doi:10.1088/1742-6596/1664/1/012016>
- [43] A. S. Al Rawas, M. Y. Slewa, B. A. Bader, N. F. Habubi, S. S. Chiad, Journal of Green Engineering, 10 (9), 7141-7153 (2020); <https://doi.org/10.1021/acsami.1c00304>
- [44] R. S. Ali, H. S. Rasheed, N. F. Habubi, S.S. Chiad, Chalcogenide Letters, 20 (1), 63–72 (2023); <https://doi.org/10.15251/CL.2023.201.63>
- [46] K. Y. Qader, R. A. Ghazi, A. M. Jabbar, K. H. Abass, S. S. Chiad, Journal of Green Engineering, 10 (10), 7387-7398, 2020. <https://doi.org/10.1016/j.jece.2020.104011>
- [47] A. Ghazai, K. Qader, N. F. Hbubi, S. S. Chiad, O. Abdulmunem, IOP Conference Series: Materials Science and Engineering, 870 (1), 012027 (2020); <https://doi.org/10.1088/1757-899X/870/1/012027>
- [48] B. A. Bader, S. K. Muhammad, A. M. Jabbar, K. H. Abass, S. S. Chiad, N. F. Habubi, J. Nanostruct, 10(4): 744-750, (2020); <https://doi.org/10.22052/JNS.2020.04.007>
- [49] O. M. Abdulmunem, A. M. Jabbar, S. K. Muhammad, M. O. Dawood, S. S. Chiad, N. F. Habubi, Journal of Physics: Conference Series, 1660 (1), 012055 (2020); <https://doi.org/10.1088/1742-6596/1660/1/012055>
- [50] R.V. Kumar, Y. Diamant, A. Gedanken, Chemistry of Materials, 12, 2301-2305(2000); <https://doi.org/10.1021/cm000166z>
- [51] E. H. Hadi, M. A. Abbsa, A. A. Khadayeir, Z. M. Abood, N. F. Habubi, and S.S. Chiad, Journal of Physics: Conference Series, 1664 (1), 012069 (2020); <https://doi.org/10.1088/1742-6596/1664/1/012069>

- [52] R. I. Jasim, E. H. Hadi, S. S. Chiad, N. F. Habubi, M. Jadan, J. S. Addasi, *Journal of Ovonic Research*, 19 (2), 187 – 196 (2023).
- [53] Salloom, H.T., Jasim, R.I., Habubi, N.F., Chiad, S.S.Jadan, M., Addasi, J.S. Gas sensor using gold doped copper oxide nanostructured thin films as modified cladding fiber, *Chinese Physics B* this link is disabled, 30(6), 068505 (2021); <https://doi.org/10.1088/1674-1056/abd2a7>
- [54] K. Y. Qader, E. H. Hadi, N. F. Habubi, S. S. Chiad, M. Jadan, J. S. Addasi, *International Journal of Thin Films Science and Technology*, 10 (1), 41-44 (2021); <https://doi.org/10.18576/ijtfst/100107>
- [55] A. Chowdhuri, V. Gupta, K. Sreenivas, R. Kumar, S. Mozumdar, P. Patanjali, *Applied Physics Letters*, 84, 1180-1182(2004); <https://doi.org/10.1063/1.1646760>